

Article pubs.acs.org/iournal/abseba

Influence of Microgel Fabrication Technique on Granular Hydrogel **Properties**

Victoria G. Muir, Taimoor H. Qazi, Junwen Shan, Jürgen Groll, and Jason A. Burdick*



Cite This: ACS Biomater. Sci. Eng. 2021, 7, 4269-4281



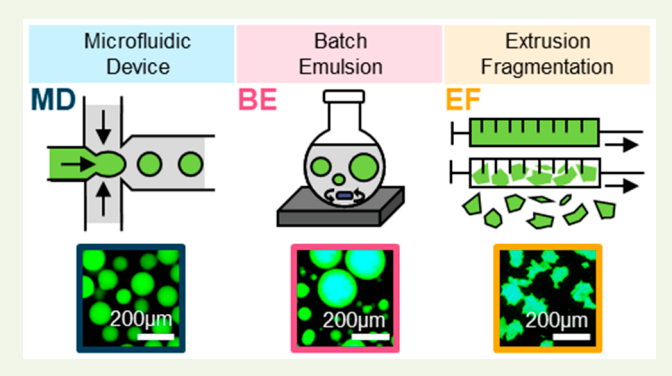
ACCESS I

Metrics & More

Article Recommendations

Supporting Information

ABSTRACT: Bulk hydrogels traditionally used for tissue engineering and drug delivery have numerous limitations, such as restricted injectability and a nanoscale porosity that reduces cell invasion and mass transport. An evolving approach to address these limitations is the fabrication of hydrogel microparticles (i.e., "microgels") that can be assembled into granular hydrogels. There are numerous methods to fabricate microgels; however, the influence of the fabrication technique on granular hydrogel properties is unexplored. Herein, we investigated the influence of three microgel fabrication techniques (microfluidic devices (MD), batch emulsions (BE), and mechanical fragmentation by extrusion (EF)) on the resulting granular hydrogel properties (e.g., mechanics, porosity, and injectability). Hyaluronic acid (HA) modified with various reactive



groups (i.e., norbornenes (NorHA), pentenoates (HA-PA), and methacrylates (MeHA)) were used to form microgels with an average diameter of ~100 µm. The MD method resulted in homogeneous spherical microgels, the BE method resulted in heterogeneous spherical microgels, and the EF method resulted in heterogeneous polygonal microgels. Across the various reactive groups, microgels fabricated with the MD and BE methods had lower functional group consumption when compared to microgels fabricated with the EF method. When microgels were jammed into granular hydrogels, the storage modulus (G') of EF granular hydrogels (\sim 1000–3000 Pa) was consistently an order of magnitude higher than G' for MD and BE granular hydrogels (\sim 50–200 Pa). Void space was comparable across all groups, although EF granular hydrogels exhibited an increased number of pores and decreased average pore size when compared to MD and BE granular hydrogels. Furthermore, granular hydrogel properties were tuned by varying the amount of cross-linker used during microgel fabrication. Lastly, granular hydrogels were injectable across formulations due to their general shear-thinning and self-healing properties. Taken together, this work thoroughly characterizes the influence of the microgel fabrication technique on granular hydrogel properties to inform the design of future systems for biomedical

KEYWORDS: hydrogels, microfluidics, microgels, granular hydrogels, hyaluronic acid, injectable

1. INTRODUCTION

Hydrogels have been widely explored for biomedical applications because of their high water content and similarities to native tissue properties. Traditional hydrogels are cross-linked in bulk, resulting in nanoscale porosity in the hydrogel mesh that permits molecular diffusion, but may limit cellular invasion without hydrogel degradation. Further, hydrogels have been processed into microporous materials, through techniques such as porogen leaching, freeze-drying, and 3D printing, which has been well covered in prior reviews.2-4 While sufficient for many applications, the combination of injectability with microscale porosity is missing with many traditional hydrogels and restricts their use in other applications. Recently, granular hydrogels have emerged as a promising biomaterial strategy to overcome many of these limitations. Granular hydrogels consist of hydrogel microparticles (i.e., "microgels") that are assembled into a jammed state, where a microscale porosity inherently exists because of the void space between microgels. 5,6 The structure of granular hydrogels allows decoupling of porosity and degradability such that cell migration, vessel infiltration, and matrix deposition are supported.^{7–9} Granular hydrogels are also inherently modular, as multiple microgel populations can be mixed and patterned to form heterogeneous scaffolds with interesting and complex properties.^{7,10} Furthermore, granular hydrogels exhibit shearthinning and self-healing behavior due to physical interactions between microgels.¹¹ Notably, interparticle cross-linking can

Special Issue: Advanced Biomedical Hydrogels

Received: November 15, 2020 Accepted: February 4, 2021 Published: February 16, 2021





also be used to form stable, annealed granular hydrogels either during processing or after injection. ^{12,13}

Given these numerous advantages, granular hydrogels have recently been explored for applications in cell culture, 1 therapeutic delivery, ¹⁶ bioprinting, ¹¹ and tissue repair. ^{12,17} As an example, microporous annealed particle (MAP) scaffolds were designed from poly(ethylene glycol) (PEG)-based microgels that were injectable, annealed by interparticle cross-linking of peptides on the microgels through Factor XIII, and supported the repair of cutaneous wounds. 12 As another example, hyaluronic acid (HA) microgels were assembled through guest-host chemical modifications to form shear-thinning granular hydrogels with mixed microgel populations for injection into myocardial tissue, where cells invaded on the basis of the selective erosion of proteasesensitive microgels.¹³ With such applications in mind for granular hydrogels, microgels can be fabricated using various methods, such as microfluidic devices, batch emulsions, and mechanical fragmentation.5

Droplet microfluidic devices have emerged as an important technique for microgel fabrication, where droplets of aqueous hydrogel precursor are formed within a continuous oil phase. Droplet size is determined mainly by the flow ratios and interfacial tension between the immiscible fluids, as well as the device channel geometry, and can range from \sim 5 to 1000 μ m in diameter. 5,18,19 Although on-chip curing is possible, droplets are typically cross-linked downstream of the microfluidic device to form stable microgels. Microgel diameters with as low as 1-2% variation have been reported using microfluidic devices.²⁰ Furthermore, complex microfluidic devices can be designed to form compartmentalized and Janus microgels, introducing opportunities for patterning and heterogeneity within single microgels.^{21–23} Microgels produced with microfluidics have previously been used as granular hydrogel inks for 3D printing and as injectable scaffolds for neural tissue repair. 11,2

Despite the precise control over microgel size and distribution with microfluidics, production rates are typically low when compared to other fabrication methods, and the time required to fabricate microgels scales with the desired volume of output. Though high-throughput microfluidic devices have been developed, ^{25,26} the production of such devices requires advanced equipment and resources, which are not widely available to all researchers. Additionally, material may be lost initially with high-throughput microfluidic devices until steady-state flow and droplet formation are achieved, which may be problematic when working with expensive biopolymers, custom synthetic polymers, and encapsulated biologics.

An alternative method to obtain spherical microgels is a batch emulsion, in which an aqueous hydrogel precursor is added to a continuous oil phase and agitated to form droplets, which are then cross-linked. Using a batch emulsion to fabricate microgels offers a few advantages over microfluidic devices, such as significantly faster production rates and the use of commonly available equipment. In addition, microgel production is limited only by vessel size and mixing ability, and agitation parameters can be tailored to alter droplet size. However, batch emulsions result in much greater distributions in microgel size when compared to microfluidic devices, with droplet diameters possibly varying by an order of magnitude within a single batch and generally ranging from ~ 1 to 1000 μ m. 5,27 The importance of monodispersity in microgel size depends on the biomedical application. For example, Xu et al.

showed that a monodisperse microgel population exhibited a sustained release of a model drug, whereas polydisperse microgels with the same mean diameter exhibited a burst release. Thorough characterization and batch repeatability may overcome size heterogeneity concerns, and postprocessing with techniques such as sieving may allow for a more monodisperse microgel population. Using batch emulsions for microgel fabrication, Truong et al. engineered HA granular hydrogel constructs for polyplex-mediated gene delivery, and Caldwell et al. investigated the influence of microgel size on secretory properties of human mesenchymal stromal cells (hMSCs) cultured in PEG granular hydrogels.

Both microfluidic devices and batch emulsions require the use of oils and surfactants to create stable emulsions, which require extensive washing steps during microgel fabrication. Exposure to harsh oils and surfactants and repeating washing can decrease cell viability if fabricating cell-laden microgels. Furthermore, if washing steps are not thorough, oils and surfactants may linger on the microgel surface, which can influence the properties and cytocompatibility of granular hydrogels. Considering this, oil-free microgel fabrication techniques have been explored. One such technique is mechanical fragmentation, where hydrogels are cross-linked in bulk and subsequently partitioned into microscale components using mechanical force, a technique that is rapid and requires few resources. Because hydrogels are polymerized in bulk, the cross-linking chemistry that is well understood for bulk hydrogels can be directly applied to microgels. Further, the size of the resulting microgels can vary from tens of micrometers through tens of millimeters in diameter, based on the extent of fragmentation. However, microgels made from mechanical fragmentation will likely be heterogeneous and irregular in shape. Using mechanical fragmentation for microgel fabrication, Sinclair et al. fabricated zwitterionic granular hydrogels on the size scale of $\sim 10-50~\mu m$ for injectable cell and therapeutic delivery,31 and Kessel et al. mechanically extruded bulk hydrogels through a grid in order to produce entangled microstrand granular hydrogels with pores between \sim 40 and 100 μ m for bioprinting.³² As another complementary method, shear has been applied during hydrogel gelation to create injectable "fluid gels" consisting of microgel particles.³³

Although the influence of microgel fabrication technique on individual microgel properties and the time and resources for microgel fabrication is now well understood, there has been little work to investigate the influence of the fabrication technique on resulting granular hydrogel properties. To better understand this relationship, we formulated HA microgels using microfluidic devices (MD), batch emulsions (BE), and mechanical fragmentation by extrusion (EF). HA was chosen because of its presence in native extracellular matrix (ECM), ease of chemical modification, and extensive documented success in biomedical applications. 34,35 To evaluate our findings across multiple cross-linking methods, we modified HA with norbornene (NorHA) or pentenoate (HA-PA) groups to form microgels through photo-cross-linkable thiol-ene radical addition, or with methacrylates (MeHA) to form microgels through photo-cross-linkable free radical kinetic chain formation. These comparisons also allow for the evaluation of whether the selected reactive group and corresponding changes in reactivity and hydrophobicity influence microgel cross-linking behavior. Microgels were formed into granular hydrogels and characterized for

rheological properties, porosity, and injectability. To our knowledge, this is the first study to directly compare properties of granular hydrogels formed from microgels made with the same materials yet different fabrication methods, offering insights into the future development of granular hydrogels for biomedical applications.

2. MATERIALS AND METHODS

- **2.1. Materials.** Sodium hyaluronic acid (HA, MW = 60 kDa) was purchased from Lifecore Biomedical. Light mineral oil and phosphate buffered saline (PBS) were purchased from Fisher Chemical. All other reagents were purchased from Sigma-Aldrich unless specified otherwise.
- **2.2.** Chemical Modification of Hyaluronic Acid (HA). Norbornene-modified HA (NorHA) was prepared as previously described. Briefly, HA modified with tetrabutylammonium salt (HA-TBA) was dissolved in anhydrous dimethyl sulfoxide (DMSO). Dimethyl aminopyridine (DMAP), norbornene carboxylic acid, and ditertbutyl dicarbonate (Boc₂O) were added to the DMSO and allowed to react overnight. NorHA product was then dialyzed for 14 days in DI water, stored at -80 °C overnight, and subsequently lyophilized for 6 days. The polymer was stored at -20 °C until further

Pentenoate-modified HA (HA-PA) synthesis was performed according to Mergy et al. 37 with slight modifications. HA was dissolved in $\rm H_2O$ (2%, $\rm w/v$) overnight at room temperature. $\rm \textit{N,N-Dimethylformamide}$ (DMF) was added to achieve a 3/2 ($\rm v/v$) mixture of $\rm H_2O/DMF$. The solution was cooled to 4 $^{\circ}C$ and pentenoic anhydride (PA, 2 eq., with respect to the repeat units of HA) was added. A solution of 1 M NaOH (1 eq., in relation to the amount of added PA) was then added, and the reaction was allowed to stir overnight and warmed to room temperature. The HA-PA product was dialyzed against distilled $\rm H_2O$ for 4 days with frequent water changes and obtained after lyophilization for 7 days.

Methacrylated HA (MeHA) was prepared as previously described. Briefly, HA was dissolved in DI water, and methacrylic anhydride was added dropwise. The pH of the reaction was maintained between 8.0 and 8.5 by adding 0.5 M NaOH dropwise over a period of 3 h. The reaction was conducted on ice and the mixture was stirred at 600 rpm. MeHA product was then dialyzed for 10 days in DI water, stored at $-80~^{\circ}\text{C}$ overnight, and subsequently lyophilized for 6 days. The polymer was stored at $-20~^{\circ}\text{C}$ until further

Lyophilized polymers were dissolved in deuterium oxide (D_2O) at a concentration of 10 mg/mL and analyzed using 1H NMR (Bruker NEO400) to determine degree of modification, which was determined to be (15 \pm 2)%, (22 \pm 2)%, and (20 \pm 1)% for NorHA, HA-PA, and MeHA, respectively.

2.3. Hydrogel Precursor Solutions and Rheological Characterization. All hydrogels and microgels were fabricated using the following precursor solutions unless otherwise indicated. NorHA hydrogels and microgels were fabricated using 3 wt % NorHA, 5 mM DTT, and 0.05 wt % Irgacure D-2959 (I2959) dissolved in PBS. HA-PA hydrogels and microgels were fabricated using 3 wt % HA-PA, 5 mM DTT, and 0.05 wt % I2959 dissolved in PBS. MeHA hydrogels and microgels were fabricated using 3 wt % MeHA and 0.1 wt % I2959 dissolved in PBS.

Rheological properties were characterized using an oscillatory shear rheometer (AR2000, TA Instruments) fitted with a 20 mm diameter cone and plate geometry and 27 μm gap. Time sweeps (0.5% strain, 1 Hz) were performed at 25 °C to characterize bulk gelation upon exposure to UV light (Omnicure S2000 lamp) for 10 min at specified intensities.

2.4. Microgel Fabrication. Microfluidic devices were fabricated using standard soft lithography. Briefly, polydimethylsiloxane (PDMS; Sylgard 184, Dow Corning) was cast onto plastic molds that were fabricated via stereolithography (Microfine green; ProtoLabs) using a custom-made design as previously reported. After overnight curing at 37 °C, the PDMS substrate was peeled away from the mold,

punched with 1 mm diameter biopsy punches (Integra Miltex) to create inlet and outlet channels, cleaned, and plasma-bonded to a standard glass slide. Stainless steel dispensing needles (19G; McMaster Carr) were inserted into the inlet and outlet channels which were then sealed using additional PDMS. Silicone tubing (Tygon; ABW00001, Saint-Gobain) was connected to the inlet and outlet needles prior to using the device.

To fabricate microgels with a microfluidic device (MD method), light mineral oil with 2 wt % Span 80 was used as the continuous phase, and microgel precursor solutions were used as the dispersed droplet phase. An oil flow rate of 150 μ L/min and a microgel precursor flow rate of 5 μ L/min were used for all macromers. Droplets were generated at the intersection point of both fluids in the microfluidic device. Droplets were exposed to UV light (Omnicure S2000) for at least 10 min while flowing through the outlet tubing and depositing into a collection vial. Light attenuation from the oil, outlet tubing, and collection vial was accounted for, and lamp settings were adjusted accordingly such that microgels experienced a UV intensity of 20 mW/cm².

To fabricate microgels with a batch emulsion (BE method), 1 mL of microgel precursor solution was added dropwise to 30 mL of light mineral oil with 2 wt % Span 80 while continuously stirring in a 100 mL round-bottom flask containing a stir bar. A mixing speed of 250 rpm was used to fabricate HA-PA and MeHA microgels and a mixing speed of 350 rpm was used for NorHA microgels, adjusted to obtain similar microgel diameters. The emulsion was exposed to UV light for 10 min while continuously stirring. Light attenuation from the oil and round-bottom flask was accounted for, and lamp settings were adjusted accordingly such that microgels experienced a UV intensity of 20 mW/cm².

Both MD and BE microgels were washed using the same protocol. Microgels were suspended in pure light mineral oil and centrifuged at 500 rpm for 2 min, and the supernatant was removed. This step was repeated 3 times. Then, microgels were incubated in PBS containing 1 wt % Tween 20 for 10 min. Microgels were centrifuged at 2000 rpm for 2 min, and the supernatant was removed. Microgels were then suspended in pure PBS and centrifuged at 2000 rpm for 2 min, and the supernatant was removed. This step was repeated 5–10 times.

To fabricate microgels by extrusion fragmentation (EF method), 1 mL of hydrogel precursor solution was added to a 3 mL syringe (BD). The syringe was exposed to UV light for 10 min. Light attenuation from the syringe was accounted for, and lamp settings were adjusted accordingly such that precursor solution experienced a UV intensity of 20 mW/cm². The bulk hydrogel was then extruded by hand through 18G, 21G, 23G, and 30G needles (McMaster-Carr), sequentially. Excess PBS (1 mL) was added after extruding through the 18G needle to reduce the extrusion forces needed. Microgels were then suspended in pure PBS and centrifuged at 2000 rpm for 2 min, and the supernatant was removed. This step was repeated three times.

- **2.5. Microgel Characterization.** Prior to fabrication, FITC-dextran (2 MDa, 0.1 wt %) was added to microgel precursor solutions. Fluorescence microscopy (Olympus BX51) was used to image the microgels after fabrication, and *ImageJ* was used to quantify microgel diameter. Specifically, for spherical microgels (MD and BE), microgel diameter was manually defined and measured. For EF microgels, microgel area was manually outlined for each particle, and the equivalent diameter of a circle of that area was used to determine the effective particle diameter. To assess the degree of consumption of reactive groups during fabrication, microgels were digested with hyaluronidase (150–600 units/mL) at 37 °C for 3 days. Digested microgels were frozen overnight at -20 °C and lyophilized for 24 h. Lyophilized product was dissolved in D₂O (10 mg/mL) and analyzed using 1 H NMR (Bruker NEO400) to determine degree of unconsumed functional groups.
- 2.6. Granular Hydrogel Formation and Rheological Characterization. Microgels suspended in PBS were jammed by vacuum-driven filtration (Steriflip, 0.22 μ m-pores, Millipore) to form granular hydrogels. Granular hydrogels were scooped with a spatula and placed on the plates of an oscillatory shear rheometer (AR2000, TA Instruments) with a 20 mm parallel plate geometry set at a 1 mm gap

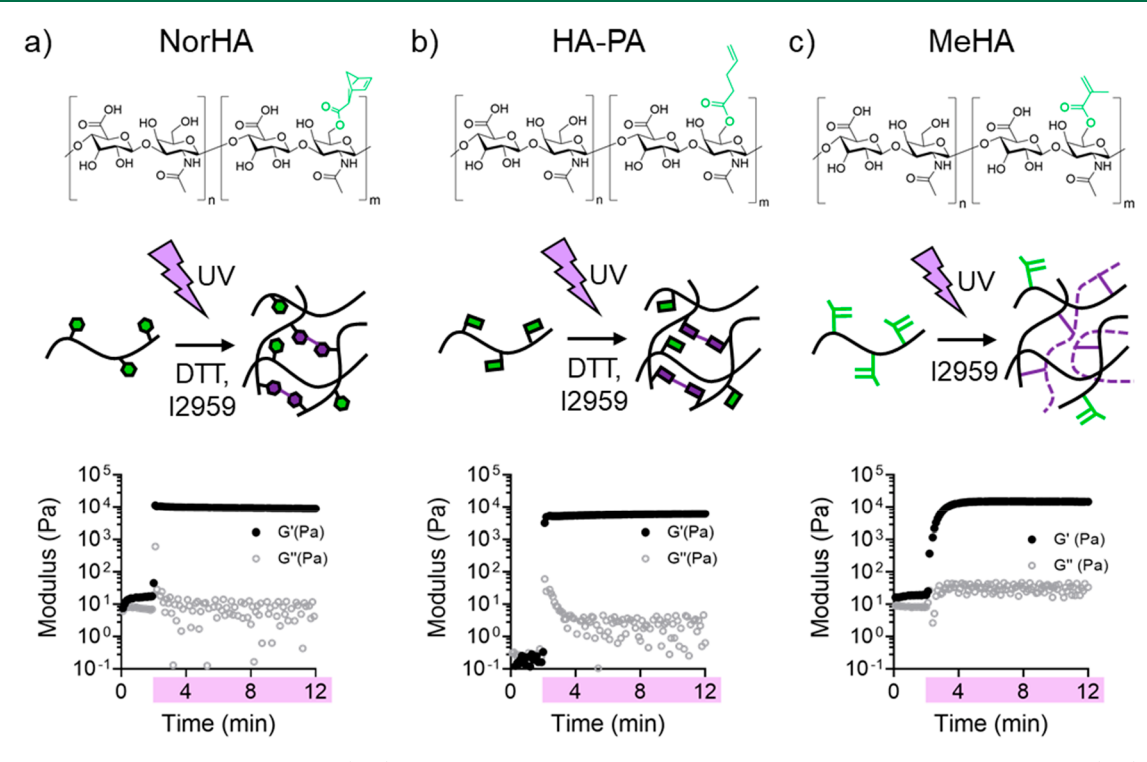


Figure 1. Chemically modified hyaluronic acid (HA) structures, cross-linking, and bulk hydrogel formation. Chemical structures (top), schematics of cross-linking (middle), and representative rheology time sweeps (1 Hz, 0.5% strain; storage [G', closed black circles] and loss [G'', open gray circles] moduli) during photo-cross-linking (bottom, purple: UV light at 20 mW/cm²) of HA modified with (a) norbornene (NorHA, $(15 \pm 2)\%$ degree of modification), (b) pentenoate (HA-PA, $(22 \pm 2)\%$ degree of modification), or methacrylate (MeHA, $(20 \pm 1)\%$ degree of modification) groups. NorHA and HA-PA undergo primarily thiol—ene radical addition photo-cross-linking (shown as line linking the reactive groups in cartoon) in the presence of dithiothreitol (DTT) and photoinitiator (Irgacure 2959, I2959), whereas MeHA undergoes photo-cross-linking through the formation of kinetic chains (shown as dotted lines) in the presence of I2959.

at 25 °C. Strain sweeps (0.5–500% strain, 1 Hz) were used to assess shear yielding properties. For flow characterization, viscosity was measured with a continuously ramped shear rate (from 0 to 50 s $^{-1}$). For shear recovery experiments, low (0.5%) and high (500%) strains were periodically applied at 1 Hz.

2.7. Confocal Imaging and Porosity Characterization. Microgels without encapsulated FITC-dextran were carefully dispersed in a 10 mg/mL solution of FITC-dextran (2 MDa) followed by jamming via vacuum-driven filtration. FITC-dextran infiltrated granular hydrogel samples were transferred to a sample holder made of a 2 mm thick PDMS slab punched with a 4 mm diameter biopsy punch and adhered onto a glass slide. Care was taken to avoid bubbles during sample transfer and to ensure complete volumetric filling of the punched sample holder. A glass coverslip was used to seal the sample to avoid dehydration. An upright confocal microscope (Leica TCS SP5) fitted with a water immersion 25× objective lens was used to visualize the FITC-Dextran distributed within the interstitial pores of the jammed granular hydrogels. Volumetric stacks measuring 500 μ m \times 500 μ m \times 100 μ m were imaged at randomly chosen regions of interest (ROI) with an average z-spacing of 5 μ m between consecutive stack slices. Porosity and pore characteristics were analyzed using FIJI ImageJ software with standard built-in functions. Briefly, images in entire stacks were converted to 8bit format, thresholded based on fluorescence, and subjected to particle analysis where each particle represented a two-dimensional pore. Reported outcomes from this analysis include percentage void fraction (porosity), number of pores, and cross-sectional area of pores, which were averaged over all images in a stack.

2.8. Compression Testing of Post-Cross-Linked Granular Hydrogels. NorHA microgels were jammed with excess I2959 and DTT. A volume of 50 μ L of granular hydrogel was secured in a cylindrical mold and exposed to UV light at an intensity of 20 mW/cm² for 5 min to form post-cross-linked constructs. Mechanical testing was performed (TA Instruments, DMA Q800) to determine the

compressive moduli of samples. Post-cross-linked granular hydrogels were secured within a fluid cup via a 0.01 N preload and compressed until failure at a rate of 0.05 N $\rm min^{-1}$. The compressive moduli were calculated as the slope from 5 to 10% strain.

2.9. Extrusion Force Measurements. Extrusion force measurements were obtained using a force sensor (Tekscan, FlexiForce Quickstart Board), myDAQ Data Acquisition Device (National Instruments), and syringe pump, as previously described. ³⁹ Granular hydrogels were loaded into a 3 mL syringe (BD) with either an 18G or 23G needle (McMaster-Carr). The syringe was loaded onto a syringe pump, and the force sensor was placed in between the plunger and syringe pump. The force sensor was connected to myDAQ for data acquisition. The syringe pump was extruded at a rate of 10 mL/min for 50 s. Voltage output was recorded using *LabView*. The extrusion force was calculated by first taking the average voltage output from the last 30 s of the 50 s extrusion time period, then comparing that average voltage to a standard force—voltage calibration curve that was created using known weights before experimentation.

2.10. Statistical Analysis. Data are presented as mean \pm standard deviation, unless otherwise indicated. Statistical analysis was conducted in *GraphPad Prism* 8 using ANOVA and a Tukey's post hoc comparison. For all samples, $n \ge 3$, *p < 0.05, **p < 0.01, ****p < 0.001, ****p < 0.001, ****p < 0.001, ****p < 0.0001, ns = not significant.

3. RESULTS AND DISCUSSION

3.1. Synthesis and Gelation Behavior of NorHA, HA-PA, and MeHA. To thoroughly understand the influence of microgel fabrication technique on granular hydrogel properties, we sought to investigate MD, BE, and EF granular hydrogels formed from multiple polymer systems. Thus, HA was modified with norbornene (NorHA), pentenoate (HA-PA), or methacrylate (MeHA) functional groups to synthesize a

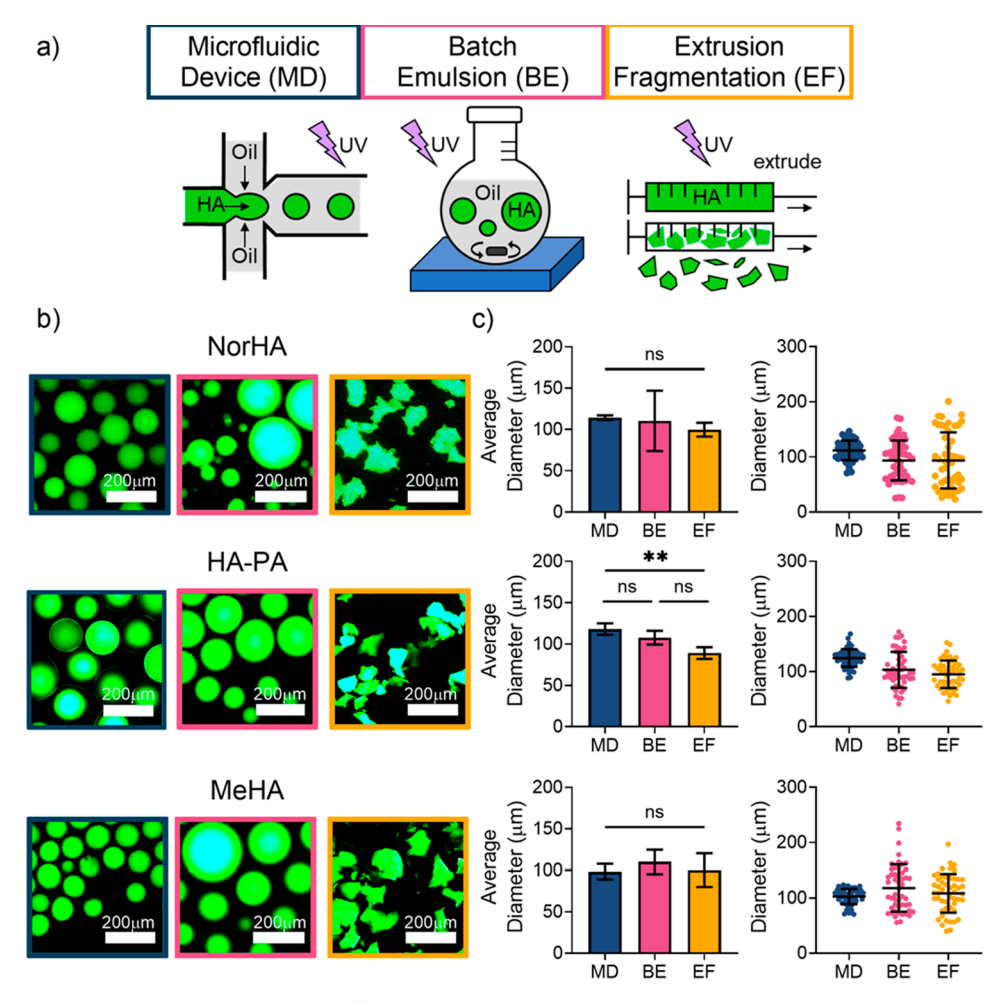


Figure 2. Microgel fabrication and size characterization. a) Schematic representation of microgels fabricated using microfluidic devices (MD, blue), batch emulsions (BE, pink), and extrusion fragmentation (EF, yellow). (b) Fluorescently labeled microgels in suspension (scale bar = 200 μ m) and (c) size quantification of NorHA (top), HA-PA (middle), and MeHA (bottom) microgels showing the average size per batch (left) and size distribution of 50 microgels within a single batch (right). For the EF method, the microgel diameter was determined by quantifying the area of a fluorescently labeled microgel in suspension and calculating an effective diameter for the area. $n \ge 3$, **p < 0.01, ns = not significant.

range of HA macromers that undergo photo-cross-linking (Figure 1). These modifications were chosen to represent a range of cross-linking chemistries, as well as functional group reactivity and hydrophobicity. The degree of modification was quantified by 1 H NMR (Figure S1) and determined to be (15 \pm 2)%, (22 \pm 2)%, and (20 \pm 1)% for NorHA, HA-PA, and MeHA, respectively. It should be noted that there are many reported modifications of HA now available, where the type of modification (e.g., covalent versus physical assembly), extent of modification, and in some cases, cross-linker used (e.g., stable versus protease-degradable peptide) can influence final material properties, such as mechanics and degradation. 34,35

To inform the microgel fabrication process, we assessed the bulk gelation properties of all three polymers with oscillatory shear photorheology with UV light (20 mW/cm²). In the presence of dithiothreitol (DTT) and a radical initiator (I2959), NorHA and HA-PA were able to photo-cross-link due to a thiol—ene radical addition between ene functionalizations (norbornene or pentenoate) on the HA macromers and thiols on DTT. In the presence of a photoinitiator (I2959), MeHA photo-cross-linked because of kinetic chain formation between methacrylate groups. Gelation occurred in less than 1 min for all three HA macromers, reaching plateau storage moduli (G') of ~10 000 Pa for NorHA and HA-PA and

 \sim 20 000 Pa for MeHA within 10 min of UV exposure. Furthermore, the rapid gelation and plateau storage moduli were also obtained within minutes even if the UV light intensity was reduced by 90% to 2 mW/cm² (Figure S2a).

Within a 10 min window of UV exposure, HA-PA was primarily cross-linked by thiol—ene radical addition. However, it is important to note that HA-PA also exhibited the ability to cross-link due to kinetic chain formation between ene groups in the absence of dithiol cross-linker, although this was much slower and results in much less cross-linking. Specifically, in the presence of I2959, but not DTT, HA-PA underwent gelation in under 10 min and reached a storage modulus of ~300 Pa after 60 min of UV exposure at an intensity of 20 mW/cm² (Figure S2b). However, given the significantly higher storage modulus and rapid gelation time in the presence of thiol crosslinkers, it is likely that thiol-ene radical addition is the dominant mechanism for cross-linking, rather than free radical kinetic chain polymerization. Moving forward, NorHA, HA-PA, and MeHA microgels were fabricated using the same precursor formulations as the bulk hydrogel studies (Figure 1), unless otherwise noted.

3.2. Microgel Fabrication and Size Characterization. Microgels were created using MD, BE, or EF methods (denoted by blue, pink, and yellow color coding, respectively),

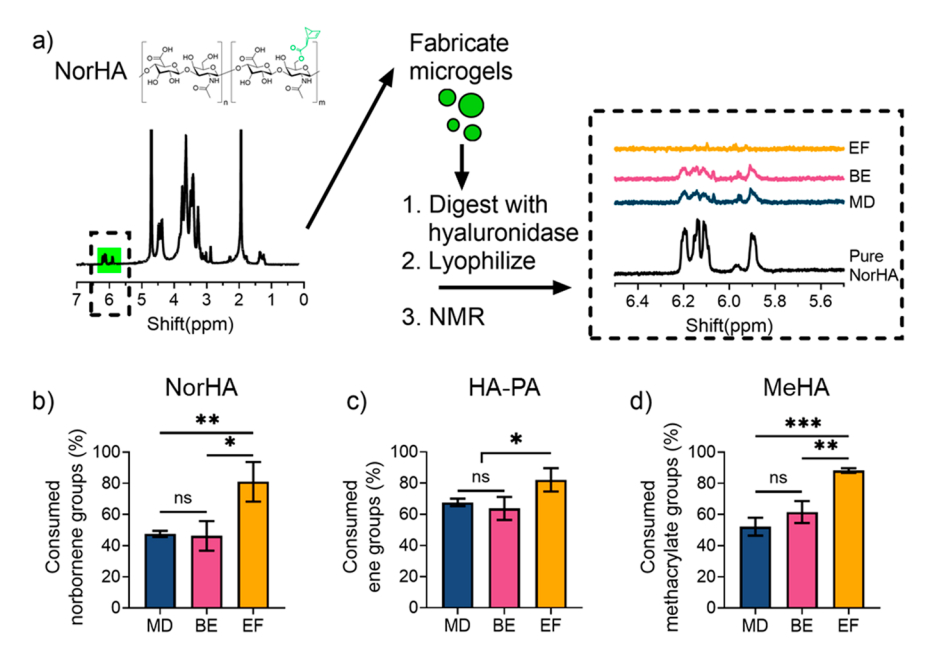


Figure 3. Degree of consumption of cross-linking groups within microgels. (a) Overview of quantification method showing a representative 1 H NMR spectrum of pure NorHA prior to microgel fabrication (left), microgel fabrication and processing steps to digest in hyaluronidase (center), and representative 1 H NMR spectra of the digested microgel showing unconsumed norbornene peaks (right). Quantified reactive group consumption during microgel fabrication using MD, BE, and EF techniques for (b) NorHA, (c) HA-PA, and (d) MeHA. $n \ge 3$, *p < 0.05, **p < 0.01, ***p < 0.001, ns = not significant.

as shown in Figure 2. Importantly, the time and resources required for each fabrication method can vary drastically. For example, with the microfluidic device and flow rates used in this study, it took around 6 h to fabricate ~1 mL of MD microgels from a prepared solution, including setup, production, and washing steps. In the BE method used in this work, these steps took around 2 h, whereas for the EF method, the processing took less than 1 h. Furthermore, the scaling of microgel volume with time should be considered with the various steps.

Microgels with a diameter around \sim 100 μ m were fabricated from NorHA, HA-PA, and MeHA using MD, BE, and EF fabrication methods where parameters (e.g., flow rate for MD, mixing speed for BE, needle gauges for EF) were adjusted to obtain similar sizes across methods (Figure 2b, c). The MD method resulted in spherical microgels that were relatively homogeneous in diameter, with a coefficient of variation of ~10-15% within a single batch across the three HA macromers investigated. Using the BE method, spherical microgels were obtained with a more heterogeneous size distribution ranging from $\sim 20-200 \, \mu \text{m}$, though still with a population average of around 100 µm. In general, the BE method resulted in microgel diameters with a coefficient of variation of ~30-40% in a single batch across the three HA macromers investigated. The EF method resulted in microgels with an irregular and jagged polygon geometry and heterogeneous size distribution across all three HA macromers, with microgel diameters ranging from \sim 20–200 μ m. The coefficient of variation for microgel diameters in a single batch ranged from ~25-50% for the EF method.

3.3. Determining Degree of Consumption of Functional Groups during Microgel Fabrication. To inform granular hydrogel design, we sought to characterize how the microgel fabrication method affects the degree of functional groups consumed during cross-linking. To solubilize the microgels after cross-linking, they were digested in hyalur-

onidase and subject to ¹H NMR analysis (Figure 3). The peaks corresponding to functional groups on the products of microgel digestion were integrated and normalized to known peaks on the HA backbone and further compared to those on the starting HA macromers. An example of the process for NorHA microgels is depicted in Figure 3a, and representative ¹H NMR spectra for each group are shown in Figure S3.

Across NorHA, HA-PA, and MeHA, a trend emerged in which the MD and BE fabrication methods resulted in decreased consumption of functional groups when compared to the EF method (Figure 3b-d). For example, NorHA precursor solutions were formulated for a theoretical 84% consumption of norbornene groups by the cross-linker DTT. In the EF method, which uses bulk hydrogel cross-linking, ~80% of norbornene groups were consumed, which is comparable to the theoretical value; however, using the same NorHA precursor solution, only ~45% of norbornene groups were consumed during cross-linking with either MD or BE fabrication methods. Similar trends in decreasing ene and methacrylate group consumption were observed for HA-PA (\sim 60%) and MeHA (\sim 55%), respectively, when the MD and BE methods were used, as compared to the EF method, where more than 80% consumption was again observed. It is important to note that, within NorHA, HA-PA, and MeHA studies, there were no significant differences observed in the degree of functional group consumption with microgels fabricated with the MD and BE methods.

During the fabrication process, with adjustments for light attenuation from the fabrication setup, UV light settings were calibrated such that microgels experienced an intensity of 20 mW/cm² across all fabrication methods. Furthermore, as shown in Figure S2a, even a 90% reduction in UV light intensity does not affect the resulting storage moduli achieved after 10 min of UV exposure for all three HA macromers when cross-linked in bulk. Thus, it is unlikely that light attenuation is responsible for observed differences in functional group

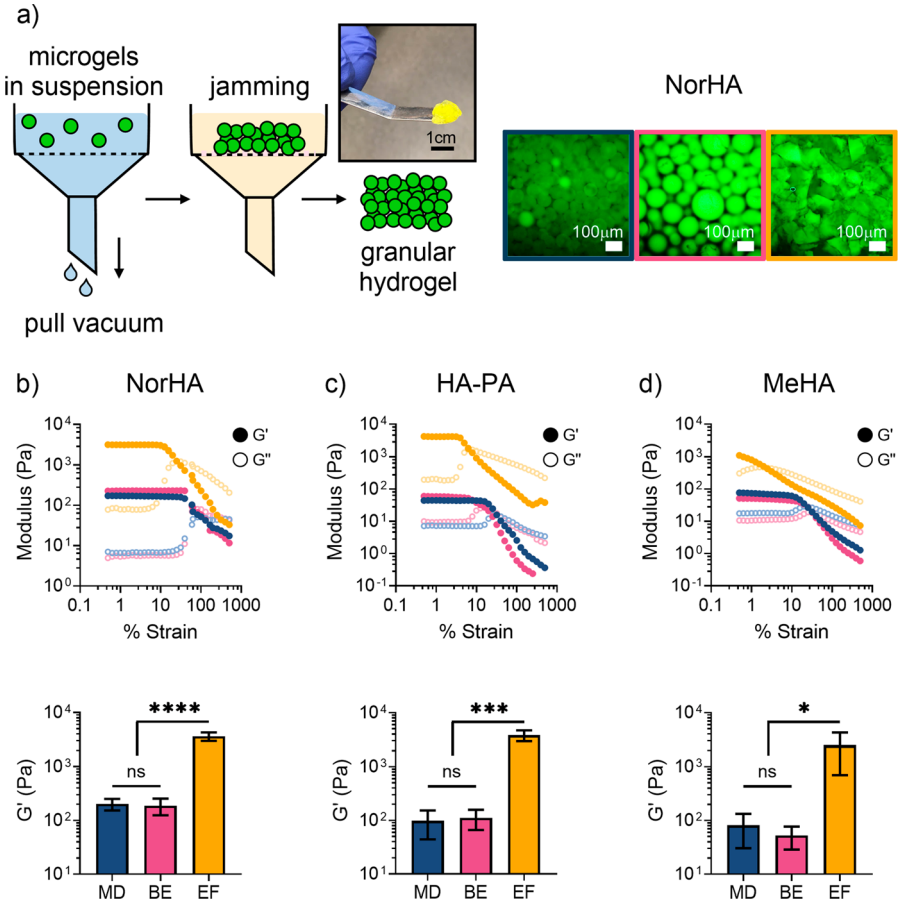


Figure 4. Granular hydrogel formation and rheological characterization. (a) Schematic of jamming microgels in suspension using vacuum filtration to form granular hydrogels with a representative macroscopic image of NorHA EF granular hydrogels on a spatula (left, scale bar = 1 cm), and representative confocal images of fluorescently labeled NorHA granular hydrogels (right, scale bar = $100 \mu m$). Quantified rheological behavior of (b) NorHA, (c) HA-PA, and (d) MeHA granular hydrogels, showing (top) shear-yielding with increasing strain (0.5–500%, 1 Hz) and (bottom) quantified storage moduli (G') of granular hydrogels at low strain (0.5%, 1 Hz). $n \ge 3$, *p < 0.05, ***p < 0.001, ****p < 0.0001, ns = not significant.

consumption during microgel fabrication. Further, for NorHA and MeHA microgels, there were no observed differences in degree of functional groups consumed when the duration of UV light exposure was increased to 100 min using the BE method (Figure S4). It is interesting to note that, for HA-PA microgels, after 100 min of UV exposure in the BE method, further consumption of functional group peaks was observed (Figure S4), likely due to cross-links from kinetic chain formation over a 60 min period (Figure S2b).

Our findings suggest that the microgel fabrication method significantly affects cross-linking during microgel fabrication, particularly with the MD and BE methods. The trend of significantly decreased functional group consumption in the MD and BE methods compared to the EF method holds true across multiple cross-linking systems, despite differences in cross-linking kinetics and functional group reactivity. There are a few major differences between microgels fabricated with the MD or BE methods and those fabricated with the EF method. First, in the MD and BE method, microscale droplets are formed before cross-linking into microgels occurs, whereas with the EF method microgels are formed by first cross-linking a bulk, macroscopic hydrogel, which is then subsequently separated into microscale microgels using mechanical force. It is possible that the microscale size influences the crosslinking behavior, as surface area to volume ratios of the

precursor solution are significantly increased when compared to a bulk hydrogel, and thus surface effects cannot be ignored. Second, microgels in the MD and BE methods are cross-linked in the presence of oil and surfactant, which are absent in the EF method. It is possible that oil and surfactant influenced the cross-linking mechanisms and kinetics of cross-linking within the microgels. Mineral oils and sorbitan surfactants, like the components used in this study, may consume nearby free radicals and decrease functional group consumption within the microgel. Ho,41 Further, mineral oil may contain dissolved oxygen, which can consume free radicals. Thus, these features likely reduce functional group consumption with MD and BE methods during microgel formation.

3.4. Rheological Properties of Granular Hydrogels. To fabricate granular hydrogels, we jammed microgels in suspension by vacuum filtration using a 0.22 μ m filter (Figure 4). Other jamming techniques such as settling or centrifugation could also be used, with various parameters (e.g., centrifuge speed) influencing the microgel packing. Granular hydrogels were fabricated from NorHA, HA-PA, and MeHA microgels fabricated using MD, BE, and EF methods. Granular hydrogels exhibited a packed particle structure, where the previous observations of microgel shape and heterogeneity were retained when visualized as granular hydrogels. All granular hydrogels exhibited shear-yielding behavior with

increased strain when examined under oscillatory shear rheology.

Across all three HA macromers, EF granular hydrogels exhibited significantly higher storage moduli (G') when compared to MD and BE granular hydrogels by 1-2 orders of magnitude. For example, NorHA granular hydrogels fabricated from MD and BE methods exhibited storage moduli around 175 Pa, whereas NorHA EF granular hydrogels exhibited a storage modulus around 3000 Pa. These results indicate that the microgel fabrication method influences the resulting granular hydrogel particles, which could be related to either the microgel geometry or the degree of consumption of reactive groups and resulting extent of cross-linking within microgels. It is important to note that no significant differences were observed with granular hydrogel moduli when fabricated from the MD and BE methods across the three HA macromers. Storage moduli were around ~175 Pa for NorHA, ~100 Pa for HA-PA, and ~75 Pa for MeHA granular hydrogels from both MD and BE methods. Based on these results, the heterogeneity in microgel diameters resulting from the BE method did not appear to significantly influence the storage moduli of the resulting granular hydrogels.

With regards to microgel shape, we hypothesize that the jagged polygon shapes of EF microgels allows for increased interdigitation of particles. This would increase resistance to shear deformation and thus result in the increased storage modulus observed in EF granular hydrogels when compared to MD and BE granular hydrogels, which are composed of spherical microgels. There have been many studies conducted to investigate the effects of particle geometry on flow properties in granular media. Many of these studies have been conducted in the field of soil science using packings of hard particles to form granular media. It has been shown through both simulation and experimental results that increasing the angularity of particles leads to a decrease in deformability of granular matter. 43-45 This may at least in part explain the significant increase in storage moduli for granular hydrogels formed from EF microgels when compared to granular hydrogels from techniques that result in spherical particles.

3.5. Porosity in Granular Hydrogels. Granular hydrogels have microscale porosity due to the void space that inherently exists between microgels after packing. Confocal microscopy was used to characterize porosity in NorHA, HA-PA, and MeHA granular hydrogels fabricated from MD, BE, and EF methods. To visualize pores, we added 2 MDa FITC-dextran to microgel suspensions, resulting in fluorescent pores after jamming. Figure 5 shows the porosity characterization for NorHA granular hydrogels, whereas the results for the HA-PA and MeHA granular hydrogel porosity characterizations are found in Figures S5 and S6, respectively. Representative images of fluorescent pores for granular hydrogels fabricated from MD, BE, and EF methods are shown in Figure 5a.

Across the three fabrication methods, the void space was <10%. NorHA granular hydrogels fabricated from the BE method resulted in the lowest void space of ~3%, and NorHA EF granular hydrogels had the highest void space of ~8%. In comparison, previous studies that use spherical microgels of similar size to form granular hydrogels have reported higher void spaces in the range 20–40%. These differences are likely caused by sample preparation techniques. Whereas other groups have relied on microgel centrifugation or microgel sedimentation followed by evaporation of the continuous

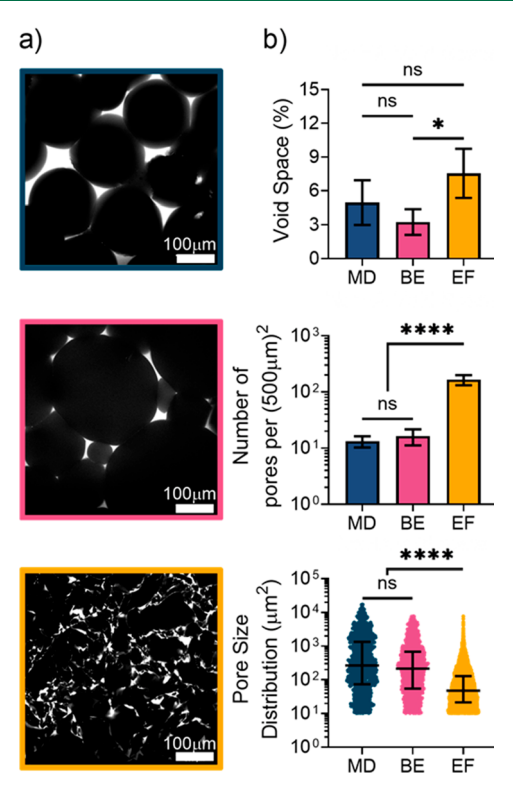


Figure 5. Porosity in NorHA granular hydrogels. (a) Representative confocal image slices of NorHA granular hydrogels, showing microgels (black) and fluorescent pores (white). Scale bar = 100 μ m. (b) Quantified porosity measurements of NorHA microgels showing void space (%) (top), number of pores per (500 μ m)² (middle), and distribution of pore sizes (bottom). Error bars in pore size distribution (bottom) show median and inner quartile ranges. $n \ge 3$ (at least 20 images were analyzed per region of interest), *p < 0.05, ****p < 0.0001, ns = not significant.

phase to form granular hydrogels,⁴⁷ our sample preparation includes vacuum-assisted removal of the continuous phase to drive jamming of microgels, forcing a tighter packing and reduced porosity.¹¹ Interestingly, although the overall void space fraction was similar across the three fabrication methods, EF granular hydrogels across all three HA macromers showed a significantly higher number of pores and a significantly lower average pore size (Figure 5b, and Figures S5 and S6). This could also partially explain the variations observed in the rheological properties mentioned in the previous section, as reduced porosity could increase the granular hydrogel storage modulus.

Although not explored in this study, the ability to tune porosity and pore characteristics, such as through the jamming technique (e.g., vacuum pressure, time of jamming), can have important implications for applying these granular hydrogels toward cell-driven tissue repair. In general, granular hydrogels support cell spreading and proliferation in vitro, and guide infiltration of cells and biological structures from surrounding tissue in vivo. ^{12,48} This void space in granular hydrogels allows cells to sense and respond to variations in biophysical and biochemical features of constituent microgels to achieve desirable cell responses such as stem cell differentiation and matrix deposition. ^{6,49,50} For example, cells respond to the surface curvature of spherical microgels by changing migration speed and gene expression, ^{30,51} which would be altered at the interface of the polygonal microgel shape and resulting pore

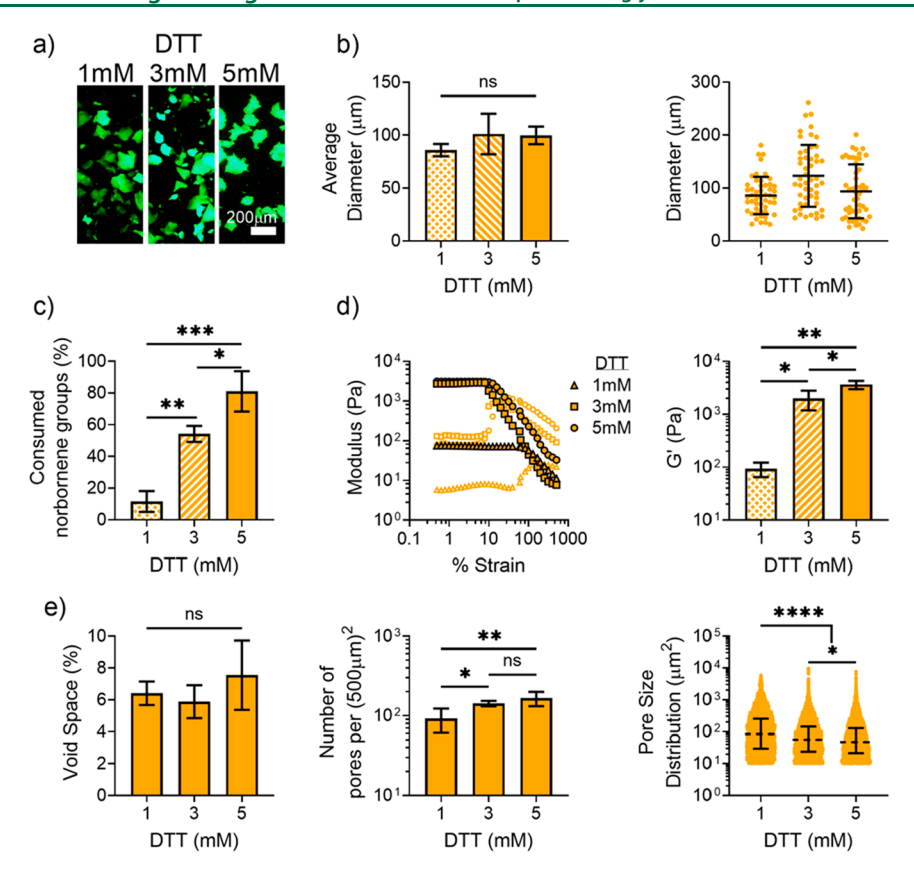


Figure 6. Tuning granular hydrogel properties by varying the extent of microgel cross-linking. NorHA granular hydrogels were formed from extrusion fragmented NorHA microgels fabricated with varied dithiothreitol (DTT) concentrations of 1, 3, and 5 mM. (a) Fluorescently labeled microgels in suspension (scale bar = 200 μ m). (b) Size characterization of microgels showing average size per batch (left) and size distribution of 50 microgels within a single batch (right). (c) Quantified ¹H NMR peak integration showing functional groups consumed during microgel fabrication. (d) Shear-yielding behavior with increasing strain (0.5–500%, 1 Hz) (left) and storage moduli (G') at low strain (0.5%, 1 Hz) (right) of granular hydrogels. (e) Quantification of porosity showing void space (%) (left), number of pores per (500 μ m)² (center), and distribution of pore sizes (right). $n \ge 3$, *p < 0.05, **p < 0.01, ***p < 0.001, ****p < 0.0001, ns = not significant.

architecture of EF granular hydrogels when compared to MD and BE hydrogels. Further tuning of granular hydrogel porosity by modifying microgel size or shape, or by modifying the processing into granular hydrogels to alter the packing density may expand the range of currently achievable pore sizes and void fractions to alter cellular interactions. ^{13,52}

3.6. Granular Hydrogels Fabricated with Varied Cross-Linker Concentrations. As the EF microgel fabrication technique allows for the rapid formation of microgels without the need for oil or surfactant, we selected this process to investigate how variation in the cross-linker concentration influences granular hydrogel properties. EF microgels were fabricated using DTT cross-linker at concentrations of 1, 3, or 5 mM (Figure 6). The average microgel size was around \sim 100 um for all three DTT concentrations (Figure 6a,b), with similar morphologies and variations between \sim 20 and 250 μ m observed within single batches across groups. ¹H NMR analysis revealed that the amount of norbornene groups consumed during the fabrication process increased with increasing DTT cross-linker concentration, closely matching the theoretical values of cross-linking of 17, 50, or 84%, for 1, 3, or 5 mM cross-linker concentration, respectively (Figure

Granular hydrogels from NorHA EF microgels with varied cross-linking all exhibited shear-yielding behavior with increased strain and the storage moduli (G') positively correlated with the amount of cross-linker, resulting in storage

moduli of 90, 1990, and 3630 Pa for 1, 3, and 5 mM DTT, respectively (Figure 6d). With regards to porosity, void space was consistently around 6–8% for each cross-linking condition investigated; however, the total number of pores increased, and average pore size decreased as a function of increasing DTT concentration. NorHA EF microgels fabricated with 1 mM DTT would likely be able to deform more easily to fill and eliminate smaller pores within the granular hydrogel structure.

It is important to note that NorHA EF microgels fabricated with 3 mM DTT have a norbornene degree of consumption of ~50%, which is similar to the degree of consumption of NorHA with MD and BE microgels fabricated with 5 mM DTT (Figure 3b). This allows for interesting comparisons, where the only measurable difference between microgels is the particle shape. Interestingly, when the degree of consumption of norbornene groups is consistent (~50%), NorHA MD and BE granular hydrogels still exhibit significantly lower storage moduli (~175 Pa) than NorHA EF granular hydrogels (~2000 Pa), by an order of magnitude. This reaffirms the impact that microgel shape has on the granular hydrogel rheological properties, as granular hydrogels from microgels of the same approximate size and cross-linking still have significantly varied storage moduli when the microgel shape is varied. However, the shape is potentially related to both the flow properties of the particles, as well as variations in porosity and packing. Microgel cross-linking will also impact the degradation behavior of the microgels. Although not investigated here,

degradation can be tuned through numerous factors, such as the type of cross-linker (e.g., hydrolysis versus protease-degradable) or mechanism of cross-linking (e.g., covalent versus physical). 34,35

To further illustrate the potential of granular hydrogels, we fabricated NorHA microgels with ~50% degree of consumption of norbornene groups (5 mM DTT for MD and BE, 3 mM DTT for EF), and subsequently processed formed granular hydrogels with a secondary cross-linking step ("postcross-linking") (Figure S7). Specifically, microgels were jammed with excess DTT and I2959 and subsequently exposed to UV light. Post-cross-linked NorHA MD and BD constructs had a compressive modulus of ~3 kPa, whereas NorHA EF constructs had a compressive modulus of \sim 10 kPa. The increase in compressive modulus observed with postcross-linked NorHA EF constructs further suggests that the jagged polygon microgel shape increases resistance to deformation when compared to spherical microgel particles. Further, EF microgels exhibit higher contact area than MD or BE microgels, as shown by the decrease in average pore size. This increase in microgel contact area may also contribute to the increased post-cross-linking observed. The use of granular hydrogels without this post-cross-linking or the introduction of post-cross-linking for further stabilization depends on the application of the granular hydrogels and desired properties. Additionally, the ability of injected microgels to migrate from the injection site, particularly without post-cross-linking, should be considered in the specific applications, as injectable microparticles on the size scale of \sim 10–100 μ m have been shown to migrate from the injection site in clinical studies. 53,54

3.7. Injectability of NorHA Granular Hydrogels. Because of their shear-thinning and self-healing properties, granular hydrogels have been explored for applications as injectable biomaterials for tissue repair and in 3D printing. As such, we sought to characterize the injectability of NorHA granular hydrogels fabricated with MD, BE, and EF methods (Figure 7). To characterize injectability, we fabricated NorHA microgels such that ~50% of norbornene groups were consumed (5 mM DTT for MD and BE, 3 mM DTT for EF). Figure 7a shows representative images of the ejection of NorHA MD, BE, and EF granular hydrogels through an 18G needle.

Across microgel fabrication methods, NorHA granular hydrogels exhibited decreased viscosity with increased shear rate (Figure 7b). NorHA EF granular hydrogels exhibited an overall increased viscosity when compared to MD and BE granular hydrogels. This is likely due to the increased angularity and interdigitation between EF microgels when compared to the spherical geometry of MD and BE microgels. Further, EF granular hydrogels exhibit decreased pore size, suggesting increased microgel contact area compared to spherical microgels in MD or BE granular hydrogels. This is important to consider given that, unlike traditional bulk hydrogels, granular hydrogels distribute force by the formation of load-bearing force chains that consist of paths of touching microparticles. 5,55 We hypothesize that increased interparticle contact area among microgels in EF granular hydrogels influences force chain formation such that resistance to shear and flow is increased when compared to MD and BE granular hydrogels.

It is interesting to note that BE granular hydrogels exhibit a slightly lower viscosity than MD granular hydrogels. In hard sphere granular media, it has been shown that more

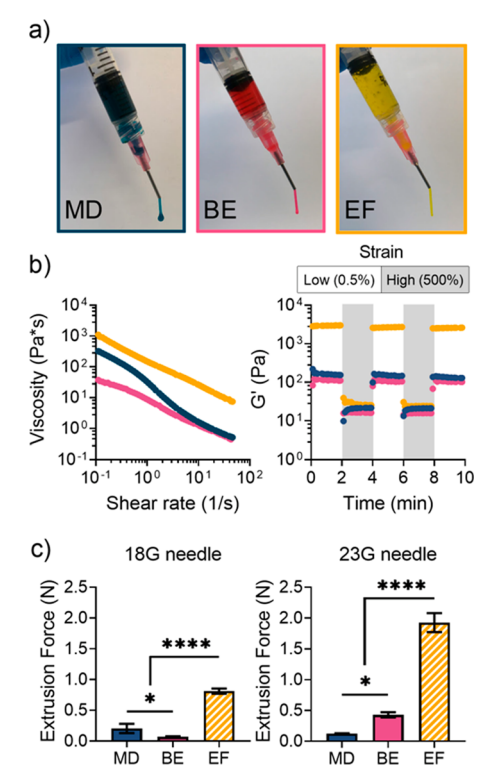


Figure 7. Injectability of NorHA granular hydrogels. (a) Representative images of extruding NorHA granular hydrogels (MD, blue; BE, pink; EF, yellow) through an 18G needle. (b) Representative rheological characterization of shear-thinning behavior through decreased viscosity with continuously increasing shear rates (0−50⁻¹ s) (left) and a rapid reduction and recover of G' with low (unshaded, 0.5% strain, 1 Hz) and high (shaded, 500% strain, 1 Hz) strain cycles (right). (c) Extrusion force measurements through an 18G (left) and 23G (right) needle at a flow rate of 10 mL/h. A DTT concentration of 3 mM was used with EF fabrication, whereas a 5 mM concentration of DTT was used for MD and BE fabrication, to maintain similar degrees of consumption (~50%). $n \ge 3$, *p < 0.05, ****p < 0.0001.

monodisperse particle populations tend to have higher relative viscosities than polydisperse particle populations.⁵⁶ The decrease in viscosity for BE granular hydrogels when compared to MD granular hydrogels may suggest that relationships in the particle size distribution and viscosity apply to the soft granular materials used herein. Furthermore, all three systems showed self-healing behavior after repeated cycles of low and high strains (Figure 7b).

As another step toward characterizing the potential injectability of granular hydrogels, the force required to extrude NorHA MD, BE, and EF granular hydrogels through an 18G and 23G needle was measured. Across the three fabrication methods, the extrusion force was well within acceptable clinical standards. 57-59 For example, it has been reported that injection forces for commercially available insulin pens can range from ~5 to 20 N,60,61 and 30 N has been considered a maximum force for manual injection.⁶² In both needle diameters, NorHA EF granular hydrogels exhibited a significantly higher extrusion force required when compared to NorHA MD and BE granular hydrogels. For BE and EF granular hydrogels, the extrusion force increased when needle inner diameter was decreased from \sim 840 μ m (18G) to \sim 340 μ m (23G). Both BE and EF microgels have a heterogeneous size distribution, and some microgels have a diameter in the

range of 200–300 μ m within each batch. These microgels may stifle flow in the 23G needle, as the microgel diameter is closer to that of the needle diameter itself. We expect that the population of larger microgels with BE and EF methods leads to the increase in extrusion force required through a 23G needle when compared to an 18G needle. There was no significant difference between the extrusion force required with 18G or 23G needles for the MD granular hydrogels. It should be noted that these measurements should be considered with respect to the specific application being used, as smaller needle diameters and more rapid injection speeds may be needed, both of which could change the force required for injection. Additionally, long catheters may be desired for other applications and measurements would need to be taken with this setup to assess feasibility.

4. CONCLUSIONS

HA microgels were fabricated from HA macromers synthesized with various reactive groups (e.g., norbornene, pentenoate, methacrylate) using microfluidic device (MD), batch emulsion (BE), and extrusion fragmentation (EF) techniques. When fabricated with similar average sizes, the fabrication method used influenced the microgel size distribution, shape, and consumption of cross-linking groups, irrespective of the reactive group added to HA. For example, the EF method resulted in irregular microgels with high reactive group consumption, whereas the MD and BE methods resulted in spherical microgels with reduced reactive group consumption. Microgels were jammed to form microporous granular hydrogels, where the resulting rheological properties, porosity, and injectability depended on the microgel fabrication technique. Specifically, EF granular hydrogels consistently showed an increased storage modulus (G') when compared to MD and BE granular hydrogels, which were relatively similar regardless of the HA macromer used. EF granular hydrogels had a significantly higher number of pores with decreased average pore size when compared to MD and BE granular hydrogels. Further, microgels across all three fabrication methods were injectable through clinically used syringe needle sizes, but the shape and size distribution notably influenced the injection forces required. Although the fabrication technique influenced granular hydrogel properties, we further showed that within a technique (e.g., EF), the various properties of granular hydrogels were easily tuned through cross-linker concentration during microgel fabrication. The results presented in this paper will have broad utility toward the improved design of injectable, modular, and microporous granular hydrogels for a variety of biomedical applications.

ASSOCIATED CONTENT

Supporting Information

The Supporting Information is available free of charge at https://pubs.acs.org/doi/10.1021/acsbiomaterials.0c01612.

Figure S1, ¹H NMR spectra of NorHA, HA-PA, and MeHA; Figure S2, rheological time sweeps of bulk gelation; Figure S3, ¹H NMR spectra of microgels; Figure S4, degree of consumption of functional groups in BE microgels after 100 min of UV exposure; Figure S5, confocal porosity analysis of HA-PA microgels; Figure S6, confocal porosity analysis of MeHA microgels; Figure S7, compression testing of post-cross-linked NorHA microgels (PDF)

AUTHOR INFORMATION

Corresponding Author

Jason A. Burdick — Department of Bioengineering, University of Pennsylvania, Philadelphia, Pennsylvania 19104, United States; orcid.org/0000-0002-2006-332X; Email: burdick2@seas.upenn.edu

Authors

Victoria G. Muir – Department of Bioengineering, University of Pennsylvania, Philadelphia, Pennsylvania 19104, United States

Taimoor H. Qazi – Department of Bioengineering, University of Pennsylvania, Philadelphia, Pennsylvania 19104, United States; orcid.org/0000-0002-3132-9170

Junwen Shan — Department of Functional Materials in Medicine and Dentistry and Bavarian Polymer Institute, University of Würzburg, 97070 Würzburg, Germany

Jürgen Groll – Department of Functional Materials in Medicine and Dentistry and Bavarian Polymer Institute, University of Würzburg, 97070 Würzburg, Germany; orcid.org/0000-0003-3167-8466

Complete contact information is available at: https://pubs.acs.org/10.1021/acsbiomaterials.0c01612

Notes

The authors declare no competing financial interest.

ACKNOWLEDGMENTS

This work was supported by the National Science Foundation (graduate research fellowship to V.G.M.), the National Institutes of Health (R01AR077362), and the German Research Foundation (postdoctoral fellowship to T.H.Q., QA 58/1-1, and collaborative research center SFB/TRR 225, project 326998133, subprojects A02 and A06). The NSF Major Research Instrumentation Program (award NSF CHE-1827457) and Vagelos Institute for Energy Science and Technology supported the purchase of the NMR machines used in this study. The authors thank Dr. Jörg Teßmar, Abhishek Dhand, Karen Xu, and Katharina Oberst for synthesis assistance, as well as Dr. Matthew Davidson, Dr. Claudia Loebel, Dr. Katrina Wisdom, Dr. Minna Chen, and Jon Galarraga for their helpful and insightful conversations.

REFERENCES

- (1) Van Vlierberghe, S.; Dubruel, P.; Schacht, E. Biopolymer-Based Hydrogels as Scaffolds for Tissue Engineering Applications: A Review. *Biomacromolecules* **2011**, *12* (5), 1387–1408.
- (2) Annabi, N.; Nichol, J. W.; Zhong, X.; Ji, C.; Koshy, S.; Khademhosseini, A.; Dehghani, F. Controlling the Porosity and Microarchitecture of Hydrogels for Tissue Engineering. *Tissue Eng., Part B* **2010**, *16* (4), 371–383.
- (3) Moroni, L.; Burdick, J. A.; Highley, C.; Lee, S. J.; Morimoto, Y.; Takeuchi, S.; Yoo, J. J. Biofabrication Strategies for 3D in Vitro Models and Regenerative Medicine. *Nat. Rev. Mater.* **2018**, 3 (5), 21–37.
- (4) Li, C.; Ouyang, L.; Armstrong, J. P. K.; Stevens, M. M. Advances in the Fabrication of Biomaterials for Gradient Tissue Engineering. *Trends Biotechnol.* **2021**, *39*, 150–164.
- (5) Daly, A. C.; Riley, L.; Segura, T.; Burdick, J. A. Hydrogel Microparticles for Biomedical Applications. *Nat. Rev. Mater.* **2020**, *5*, 20.
- (6) Riley, L.; Schirmer, L.; Segura, T. Granular Hydrogels: Emergent Properties of Jammed Hydrogel Microparticles and Their Applica-

- tions in Tissue Repair and Regeneration. *Curr. Opin. Biotechnol.* **2019**, 60, 1–8.
- (7) de Rutte, J. M.; Koh, J.; Di Carlo, D. Scalable High-Throughput Production of Modular Microgels for In Situ Assembly of Microporous Tissue Scaffolds. *Adv. Funct. Mater.* **2019**, 29 (25), 1970174.
- (8) Sideris, E.; Griffin, D. R.; Ding, Y.; Li, S.; Weaver, W. M.; Di Carlo, D.; Hsiai, T.; Segura, T. Particle Hydrogels Based on Hyaluronic Acid Building Blocks. *ACS Biomater. Sci. Eng.* **2016**, 2 (11), 2034–2041.
- (9) Sheikhi, A.; de Rutte, J.; Haghniaz, R.; Akouissi, O.; Sohrabi, A.; Di Carlo, D.; Khademhosseini, A. Microfluidic-Enabled Bottom-up Hydrogels from Annealable Naturally-Derived Protein Microbeads. *Biomaterials* **2019**, 192, 560–568.
- (10) Darling, N. J.; Sideris, E.; Hamada, N.; Carmichael, S. T.; Segura, T. Injectable and Spatially Patterned Microporous Annealed Particle (MAP) Hydrogels for Tissue Repair Applications. *Adv. Sci.* **2018**, *5* (11), 1801046.
- (11) Highley, C. B.; Song, K. H.; Daly, A. C.; Burdick, J. A. Jammed Microgel Inks for 3D Printing Applications. *Adv. Sci.* **2019**, *6* (1), 1801076.
- (12) Griffin, D. R.; Weaver, W. M.; Scumpia, P. O.; Di Carlo, D.; Segura, T. Accelerated Wound Healing by Injectable Microporous Gel Scaffolds Assembled from Annealed Building Blocks. *Nat. Mater.* **2015**, *14* (7), 737–744.
- (13) Mealy, J. E.; Chung, J. J.; Jeong, H. H.; Issadore, D.; Lee, D.; Atluri, P.; Burdick, J. A. Injectable Granular Hydrogels with Multifunctional Properties for Biomedical Applications. *Adv. Mater.* **2018**, *30* (20), 1705912.
- (14) Li, F.; Truong, V. X.; Fisch, P.; Levinson, C.; Glattauer, V.; Zenobi-Wong, M.; Thissen, H.; Forsythe, J. S.; Frith, J. E. Cartilage Tissue Formation through Assembly of Microgels Containing Mesenchymal Stem Cells. *Acta Biomater.* **2018**, *77*, 48–62.
- (15) Caldwell, A. S.; Rao, V. V.; Golden, A. C.; Anseth, K. S. Porous Bio-Click Microgel Scaffolds Control HMSC Interactions and Promote Their Secretory Properties. *Biomaterials* **2020**, 232, 119725.
- (16) Chen, M. H.; Chung, J. J.; Mealy, J. E.; Zaman, S.; Li, E. C.; Arisi, M. F.; Atluri, P.; Burdick, J. A. Injectable Supramolecular Hydrogel/Microgel Composites for Therapeutic Delivery. *Macromol. Biosci.* **2019**, *19* (1), 1800248.
- (17) Nih, L. R.; Sideris, E.; Carmichael, S. T.; Segura, T. Injection of Microporous Annealing Particle (MAP) Hydrogels in the Stroke Cavity Reduces Gliosis and Inflammation and Promotes NPC Migration to the Lesion. *Adv. Mater.* **2017**, *29* (32), 1606471.
- (18) Dendukuri, D.; Tsoi, K.; Hatton, T. A.; Doyle, P. S. Controlled Synthesis of Nonspherical Microparticles Using Microfluidics. *Langmuir* **2005**, *21* (6), 2113–2116.
- (19) Sohrabi, S.; Kassir, N.; Keshavarz Moraveji, M. Droplet Microfluidics: Fundamentals and Its Advanced Applications. *RSC Adv.* **2020**, *10* (46), 27560–27574.
- (20) Nisisako, T.; Torii, T. Microfluidic Large-Scale Integration on a Chip for Mass Production of Monodisperse Droplets and Particles. *Lab Chip* **2008**, 8 (2), 287–293.
- (21) Chu, L. Y.; Utada, A. S.; Shah, R. K.; Kim, J. W.; Weitz, D. A. Controllable Monodisperse Multiple Emulsions. *Angew. Chem., Int. Ed.* **2007**, *46* (47), 8970–8974.
- (22) Utada, A. S.; Lorenceau, E.; Link, D. R.; Kaplan, P. D.; Stone, H. A.; Weitz, D. A. Monodisperse Double Emulsions Generated from a Microcapillary Device. *Science (Washington, DC, U. S.)* **2005**, 308 (5721), 537–541.
- (23) Seiffert, S.; Romanowsky, M. B.; Weitz, D. A. Janus Microgels Produced from Functional Precursor Polymers. *Langmuir* **2010**, *26* (18), 14842–14847.
- (24) Hsu, R. S.; Chen, P. Y.; Fang, J. H.; Chen, Y. Y.; Chang, C. W.; Lu, Y. J.; Hu, S. H. Adaptable Microporous Hydrogels of Propagating NGF-Gradient by Injectable Building Blocks for Accelerated Axonal Outgrowth. *Adv. Sci.* **2019**, *6* (16), 1900520.
- (25) Headen, D. M.; García, J. R.; García, A. J. Parallel Droplet Microfluidics for High Throughput Cell Encapsulation and Synthetic Microgel Generation. *Microsystems Nanoeng.* **2018**, *4* (1), 1–9.

- (26) Bardin, D.; Kendall, M. R.; Dayton, P. A.; Lee, A. P. Parallel Generation of Uniform Fine Droplets at Hundreds of Kilohertz in a Flow-Focusing Module. *Biomicrofluidics* **2013**, *7* (3), 034112.
- (27) Darling, N. J.; Xi, W.; Sideris, E.; Anderson, A. R.; Pong, C.; Carmichael, S. T.; Segura, T. Click by Click Microporous Annealed Particle (MAP) Scaffolds. *Adv. Healthcare Mater.* **2020**, *9* (10), 1901391.
- (28) Xu, Q.; Hashimoto, M.; Dang, T. T.; Hoare, T.; Kohane, D. S.; Whitesides, G. M.; Langer, R.; Anderson, D. G. Preparation of Monodisperse Biodegradable Polymer Microparticles Using a Microfluidic Flow-Focusing Device for Controlled Drug Delivery. *Small* **2009**, *5* (13), 1575–1581.
- (29) Truong, N. F.; Lesher-Pérez, S. C.; Kurt, E.; Segura, T. Pathways Governing Polyethylenimine Polyplex Transfection in Microporous Annealed Particle Scaffolds. *Bioconjugate Chem.* **2019**, 30 (2), 476–486.
- (30) Truong, N. F.; Kurt, E.; Tahmizyan, N.; Lesher-Pérez, S. C.; Chen, M.; Darling, N. J.; Xi, W.; Segura, T. Microporous Annealed Particle Hydrogel Stiffness, Void Space Size, and Adhesion Properties Impact Cell Proliferation, Cell Spreading, and Gene Transfer. *Acta Biomater.* **2019**, *94*, 160–172.
- (31) Sinclair, A.; O'Kelly, M. B.; Bai, T.; Hung, H. C.; Jain, P.; Jiang, S. Self-Healing Zwitterionic Microgels as a Versatile Platform for Malleable Cell Constructs and Injectable Therapies. *Adv. Mater.* **2018**, 30 (39), 1870291.
- (32) Kessel, B.; Lee, M.; Bonato, A.; Tinguely, Y.; Tosoratti, E.; Zenobi-Wong, M. 3D Bioprinting of Macroporous Materials Based on Entangled Hydrogel Microstrands. *Adv. Sci.* **2020**, *7*, 2001419.
- (33) Cooke, M. E.; Jones, S. W.; ter Horst, B.; Moiemen, N.; Snow, M.; Chouhan, G.; Hill, L. J.; Esmaeli, M.; Moakes, R. J. A.; Holton, J.; Nandra, R.; Williams, R. L.; Smith, A. M.; Grover, L. M. Structuring of Hydrogels across Multiple Length Scales for Biomedical Applications. *Adv. Mater.* **2018**, *30* (14), e1705013.
- (34) Burdick, J. A.; Prestwich, G. D. Hyaluronic Acid Hydrogels for Biomedical Applications. *Adv. Mater.* **2011**, 23 (12), 41–56.
- (35) Highley, C. B.; Prestwich, G. D.; Burdick, J. A. Recent Advances in Hyaluronic Acid Hydrogels for Biomedical Applications. *Curr. Opin. Biotechnol.* **2016**, *40*, 35–40.
- (36) Gramlich, W. M.; Kim, I. L.; Burdick, J. A. Synthesis and Orthogonal Photopatterning of Hyaluronic Acid Hydrogels with Thiol-Norbornene Chemistry. *Biomaterials* **2013**, 34 (38), 9803–9811.
- (37) Mergy, J.; Fournier, A.; Hachet, E.; Auzély-Velty, R. Modification of Polysaccharides via Thiol-Ene Chemistry: A Versatile Route to Functional Biomaterials. *J. Polym. Sci., Part A: Polym. Chem.* **2012**, *50* (19), 4019–4028.
- (38) Loebel, C.; Rodell, C. B.; Chen, M. H.; Burdick, J. A. Shear-Thinning and Self-Healing Hydrogels as Injectable Therapeutics and for 3D-Printing. *Nat. Protoc.* **2017**, *12* (8), 1521–1541.
- (39) Chen, M. H.; Wang, L. L.; Chung, J. J.; Kim, Y. H.; Atluri, P.; Burdick, J. A. Methods to Assess Shear-Thinning Hydrogels for Application As Injectable Biomaterials. *ACS Biomater. Sci. Eng.* **2017**, 3 (12), 3146–3160.
- (40) Ambrosone, L.; Mosca, M.; Ceglie, A. Impact of Edible Surfactants on the Oxidation of Olive Oil in Water-in-Oil Emulsions. *Food Hydrocolloids* **2007**, *21* (7), 1163–1171.
- (41) Otsuki, J.; Nagai, Y.; Chiba, K. Peroxidation of Mineral Oil Used in Droplet Culture Is Detrimental to Fertilization and Embryo Development. *Fertil. Steril.* **2007**, *88* (3), 741–743.
- (42) Englander, S. W.; Calhoun, D. B.; Englander, J. J. Biochemistry without Oxygen. *Anal. Biochem.* **1987**, *161* (2), 300–306.
- (43) Robinson, D. A.; Friedman, S. P. Observations of the Effects of Particle Shape and Particle Size Distribution on Avalanching of Granular Media. *Phys. A* **2002**, *311* (1–2), 97–110.
- (44) Nouguier-Lehon, C.; Cambou, B.; Vincens, E. Influence of Particle Shape and Angularity on the Behaviour of Granular Materials: A Numerical Analysis. *Int. J. Numer. Anal. Methods Geomech.* **2003**, *27* (14), 1207–1226.

- (45) Afzali-Nejad, A.; Lashkari, A.; Shourijeh, P. T. Influence of Particle Shape on the Shear Strength and Dilation of Sand-Woven Geotextile Interfaces. *Geotext. Geomembranes* **2017**, *45* (1), 54–66.
- (46) Caldwell, A. S.; Campbell, G. T.; Shekiro, K. M. T.; Anseth, K. S. Clickable Microgel Scaffolds as Platforms for 3D Cell Encapsulation. *Adv. Healthcare Mater.* **2017**, *6* (15), 1–8.
- (47) Xin, S.; Dai, J.; Gregory, C. A.; Han, A.; Alge, D. L. Creating Physicochemical Gradients in Modular Microporous Annealed Particle Hydrogels via a Microfluidic Method. *Adv. Funct. Mater.* **2020**, 30 (6), 1907102.
- (48) Fang, J.; Koh, J.; Fang, Q.; Qiu, H.; Archang, M. M.; Hasani-Sadrabadi, M. M.; Miwa, H.; Zhong, X.; Sievers, R.; Gao, D. W.; Lee, R.; Di Carlo, D.; Li, S. Injectable Drug-Releasing Microporous Annealed Particle Scaffolds for Treating Myocardial Infarction. *Adv. Funct. Mater.* **2020**, 30, 2070289.
- (49) Koh, J.; Griffin, D. R.; Archang, M. M.; Feng, A. C.; Horn, T.; Margolis, M.; Zalazar, D.; Segura, T.; Scumpia, P. O.; Di Carlo, D. Enhanced In Vivo Delivery of Stem Cells Using Microporous Annealed Particle Scaffolds. *Small* **2019**, *15* (39), e1903147.
- (50) Caldwell, A. S.; Aguado, B. A.; Anseth, K. S. Designing Microgels for Cell Culture and Controlled Assembly of Tissue Microenvironments. *Adv. Funct. Mater.* **2020**, *30*, 1907670.
- (51) Werner, M.; Blanquer, S. B. G.; Haimi, S. P.; Korus, G.; Dunlop, J. W. C.; Duda, G. N.; Grijpma, D. W.; Petersen, A. Surface Curvature Differentially Regulates Stem Cell Migration and Differentiation via Altered Attachment Morphology and Nuclear Deformation. *Adv. Sci.* **2017**, *4* (2), 1–11.
- (52) Draghi, L.; Resta, S.; Pirozzolo, M. G.; Tanzi, M. C. Microspheres Leaching for Scaffold Porosity Control. *J. Mater. Sci.: Mater. Med.* **2005**, *16* (12), 1093–1097.
- (53) Malizia, A. A.; Reiman, H. M.; Myers, R. P.; Sande, J. R.; Barham, S. S.; Benson, R. C.; Dewanjee, M. K.; Utz, W. J. Migration and Granulomatous Reaction After Periurethral Injection of Polytef (Teflon). *JAMA J. Am. Med. Assoc.* **1984**, 251 (24), 3277–3281.
- (54) Vidart, A.; Zimmern, P. E. Migration of Durasphere after Transurethral Injection for Stress Urinary Incontinence. *J. Pelvic Med. Surg.* **2004**, *10* (1), 39–40.
- (\$\$) Furbish, D. J.; Schmeeckle, M. W.; Roering, J. J. Thermal and Force-Chain Effects in an Experimental, Sloping Granular Shear Flow. *Earth Surf. Processes Landforms* **2008**, 33, 2108–2117.
- (56) Luckham, P. F.; Ukeje, M. A. Effect of Particle Size Distribution on the Rheology of Dispersed Systems. *J. Colloid Interface Sci.* 1999, 220 (2), 347–356.
- (57) Peebles, L.; Norris, B. Filling "gaps" in Strength Data for Design. Appl. Ergon. 2003, 34 (1), 73–88.
- (58) Vo, A.; Doumit, M.; Rockwell, G. The Biomechanics and Optimization of the Needle-Syringe System for Injecting Triamcinolone Acetonide into Keloids. *J. Med. Eng.* **2016**, *2016*, *1*–8.
- (59) Kappes, C. M.; Kershner, J. R.; Morwick, T. M.; Corrigan, S. M. Dose Accuracy, Injection Force, and Usability Assessment of a New Half-Unit, Prefilled Insulin Pen. J. Diabetes Sci. Technol. 2018, 12 (2), 364–372.
- (60) Van Der Burg, T. Injection Force of SoloSTAR® Compared with Other Disposable Insulin Pen Devices at Constant Volume Flow Rates. *J. Diabetes Sci. Technol.* **2011**, *5* (1), 150–155.
- (61) Pfützner, A.; Reimer, T.; Hohberg, C.; Frøkjæer, L. P. F.; Jørgensen, C. Prefilled Insulin Device with Reduced Injection Force: Patient Perception and Accuracy. *Curr. Med. Res. Opin.* **2008**, 24 (9), 2545–2549.
- (62) Burckbuchler, V.; Mekhloufi, G.; Giteau, A. P.; Grossiord, J. L.; Huille, S.; Agnely, F. Rheological and Syringeability Properties of Highly Concentrated Human Polyclonal Immunoglobulin Solutions. *Eur. J. Pharm. Biopharm.* **2010**, *76* (3), 351–356.